

Many-body calculation of the spatial extent of the wave-function of a non-magnetic impurity in a d-wave high-temperature superconductor using the t - J model

Manuela Capello¹ and Didier Poilblanc^{2,1}

¹*Laboratoire de Physique Théorique, CNRS and Université de Toulouse, F-31062 Toulouse, France*

²*Institute of Theoretical Physics, Ecole Polytechnique Fédérale de Lausanne, CH-1015 Lausanne, Switzerland*

(Dated: November 8, 2018)

Scanning tunneling microscopy (STM) by providing images of the effects of individual zinc-impurities in cuprate superconductors with unprecedented atomic-resolution offers a stringent test to models of correlated fermions for high-temperature superconductors. Using a t - J model supplemented by Variational Monte Carlo many-body techniques, the spatial dependence of the hole density and of the valence bond and superconducting pairing amplitudes around the impurity are computed. A cross-shaped four-fold symmetric structure very similar to the observed STM observation is found, giving strong credit to the model.

Introduction – Cuprates superconductors can be considered as doped two-dimensional (2D) Mott insulators where electronic correlations play a dominant role^{1,2}. A number of exotic properties such as the pseudo-gap behavior reflect the complexity of the system. In a pioneering work, Anderson proposed the Resonating Valence Bond (RVB) Mott insulator as the relevant underlying *parent* state³ from which gapless d-wave superconductivity naturally emerges under doping. Within this scenario, the pseudo-gap naturally emerges as the energy scale associated to the formation of singlet electron pairs via the nearest-neighbor antiferromagnetic (AF) exchange. A mean-field version of the RVB theory using a t - J model¹ could also explain a number of bulk experimental observations⁴.

Local probes of correlated materials with atomic resolution have recently become possible thanks to Scanning Tunneling Microscopy (STM)⁵ which provided unprecedented high-resolution maps of the surface of some underdoped cuprate superconductors⁶. The measured space-resolved doped-hole charge density in the SC regime of Na-CCOC and Dy-Bi2212 cuprates revealed stripe patterns⁷. This discovery naturally raises the question whether such inhomogeneities are induced by impurities or whether they are intrinsic as the bulk static charge and spin stripe orders detected in Nd-LSCO⁸ and LBCO⁹ cuprates at doping $\delta \sim 1/8$.

Substituting a single impurity atom for a copper atom indeed strongly affects its surrounding region. Therefore, it can serve as a local fine probe, providing important insights about the properties of the correlated medium itself¹⁰. Imaging the effects of individual zinc impurity atoms on superconducting Bi2212 performed by STM¹¹ showed clear real-space modulations which can be confronted to theoretical modeling. In other words, such observations offer a new stringent test to models of correlated fermions for high-temperature superconductors. It has been argued that a number of bulk properties of these materials can be explained within the correlated t - J model¹². However, local real-space responses have not yet been calculated reliably since, due to the short superconducting coherence length, a fully many-body ap-

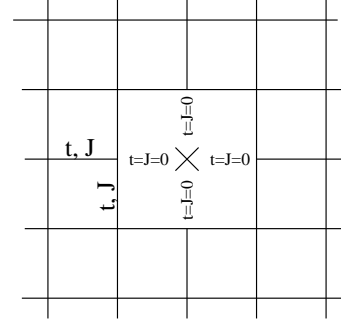


FIG. 1: Schematic representation of the impurity model. The cross corresponds to the impurity site i_0 . The parameters t and J are set to zero on the four bonds connected to the impurity site.

proach is needed. In this Letter, we have carried out such a program of (i) computing within a many-body numerical technique the response induced by the introduction of a spinless impurity site within a bulk two-dimensional t - J model and (ii) confronting the theoretical results to the experimental observations to validate or invalidate the model.

The $t - J$ Hamiltonian on a square lattice reads,

$$H_{t-J} = - \sum_{\langle i,j \rangle \sigma} t_{ij} (c_{i\sigma}^\dagger c_{j\sigma} + h.c.) + \sum_{\langle i,j \rangle} J_{ij} S_i \cdot S_j. \quad (1)$$

A zinc impurity is in the same 2+ oxidation state as the copper ion it is substituted for, so that it does not introduce extra charge. However, in contrast to the copper $S=1/2$ ion, the Zn^{2+} ion is in a spin-singlet state, inert magnetically. Hence, one can use a simple description : on the four bonds connected to the impurity site we set $t_{ij} = 0$ and $J_{ij} = 0$ as shown on Fig. 1. On all the other bonds, we set t_{ij} and J_{ij} to the same values t and J , respectively. Although completely local such a "boundary" is expected to lead to a *spatially-extended* perturbation strongly affecting GS properties.

Description of method – Variational fully-projected fermionic wave-functions¹³ (WF) are known to incor-

porate very satisfactorily correlation effects of the t - J model. We have extended them to finite periodic $L \times L$ clusters containing a single impurity (in practice, $L = 8$ and $L = 16$). A Variational Monte Carlo (VMC) scheme¹³ is used to (i) realize a thorough optimization over the variational parameters¹⁴ (see below) and (ii) to calculate the ground-state (GS) physical observables. The presence of the impurity on site i_0 modifies the Hilbert space, i.e. $c_{i_0\sigma}^\dagger|\Psi\rangle = 0$ and $c_{i_0\sigma}|\Psi\rangle = 0$, where $|\Psi\rangle$ is the GS of the system. In our Monte Carlo variational scheme an ‘‘impurity projector’’ $\mathcal{P}_{i_0} = (1 - n_{i_0\uparrow})(1 - n_{i_0\downarrow})$ is inserted, and the impurity variational wavefunction is defined as $|\Psi_{\text{VMC}}\rangle = \mathcal{P}_g \mathcal{P}_{i_0} |D\rangle$, where \mathcal{P}_g is the usual Gutzwiller projector enforcing the constraint of no-double occupancy on the remaining $L^2 - 1$ sites.

Motivated by the success of the RVB theory to explain bulk properties⁴ the mean-field determinant $|D\rangle$ is chosen to be the ground-state of a mean-field Hamiltonian of standard BCS-type,

$$H_{\text{MF}} = \sum_{\langle i,j \rangle \sigma} (\chi_{ij} c_{i\sigma}^\dagger c_{j\sigma} + h.c.) + \sum_{\langle i,j \rangle} (\Delta_{ij} c_{i\uparrow}^\dagger c_{j\downarrow}^\dagger + h.c.) + \mu \sum_{i\sigma} n_{i\sigma}, \quad (2)$$

defined on *all* of the $L \times L$ sites, including the i_0 site (always occupied by a hole). We optimize *all* different non-equivalent bonds around the impurity, starting from an initial guess respecting or not the square lattice symmetry around i_0 . Since in principle the Hamiltonian C_{4v} symmetry around i_0 (see Figure 1) could be spontaneously broken, we have performed a number of preliminary tests on small 8×8 lattices, choosing the initial RVB bonds pattern with lower symmetries like e.g. C_4 or C_{2v} symmetries (the later allowing the formation of a domain wall). We have found that the full C_{4v} symmetry is systematically restored at the variational minimum. Therefore, to reduce the number of variational parameters and gain accuracy, the C_{4v} symmetry has been enforced on our largest 16×16 cluster. As expected, all optimized WFs are found to show opposite signs of Δ_{ij} on any site-sharing vertical and horizontal bonds, hence reflecting the expected *orbital d-wave character* of the superconducting order. Lastly, we note that allowing *finite* values of the parameters Δ_{ij} and χ_{ij} on the four bonds connected to the impurity is also important to gain energy as shown on Table I. The lowest-energy state (II) is obtained for a full optimization of the Δ_{ij} and χ_{ij} parameters over *all bonds*. Typically, χ_{ij} has a significant magnitude on the four bonds connected to the impurity site. Moreover, for decreasing doping, a sizable amplitude of Δ_{ij} also appears on the later bonds.

Results on 16×16 clusters – We now turn to the VMC calculations on the 16×16 cluster with periodic-boundary conditions, assuming a physical value of $t/J = 3$. Here, we consider a physical ‘‘core’’ 8×8 region centered around the impurity (i.e. of the same size as our previous small cluster), where we impose a C_{4v} symmetry around

TABLE I: Variational energy per site (in units of t) for different projected WFs for the t - J model at doping $1/8$ ($N_h = 8$), for $t/J = 3$ and a 8×8 cluster with an impurity. (I) $|D(8 \times 8)\rangle$ is optimized fixing $\Delta_{ij} = 0$, $\chi_{ij} = 0$ around the impurity and $\mu_{i_0} = 0$. Everywhere else Δ_{ij} optimized and $\chi_{ij} = 1$; (II) $|D(8 \times 8)\rangle$ is fully optimized with all possible Δ_{ij} and χ_{ij} (including the impurity bonds). The (total) energy difference between (I) and (II) is $\sim 0.3t$ per impurity.

$ D\rangle$:	(I)	(II)
$E_{\text{VMC}}[t]$:	-0.41493(5)	-0.41968(5)

the impurity site. Outside, we assume a uniform d -wave superconducting background (bg) whose parameters $\chi_{i,i+\hat{x}} = \chi_{i,i+\hat{y}} = \chi_{\text{bg}}$ and $\Delta_{i,i+\hat{x}} = -\Delta_{i,i+\hat{y}} = \Delta_{\text{bg}}$ are optimized simultaneously. This enables to reduce significantly the boundary effects and is justified since the spatial extension of the effect of the impurity rarely exceeds the assumed size of the core.

The spacial distribution of the local hole density $\langle c_{i\sigma} c_{i\sigma}^\dagger \rangle$, the bond hole kinetic amplitudes $K_{ij} = \langle (c_{j\sigma} c_{i\sigma}^\dagger + h.c.) \rangle$ and the magnetic VB amplitudes $S_{ij} = \langle \mathbf{S}_i \cdot \mathbf{S}_j \rangle$ are shown in Fig. 2(a) and in Fig. 3(a), respectively, for doping $1/8$. Here, and throughout the paper, we only show the 6×6 central region exhibiting the largest modulations. It turns out that the variational parameters Δ_{ij} are suppressed on the four bonds connected to the impurity. This is compensated by an increase in Δ_{ij} and hence of S_{ij} on the neighboring bonds, forming a cross-like structure (see thick blue bonds of Fig. 3(a)). Due to similarities with work done in a somewhat different context¹⁷, we shall refer to these bonds as the four ‘‘dimer bonds’’. These bonds are characterized by a simultaneous hole deficiency and a large gain in the magnetic energy (which can reach more than 40%), hence signaling a tendency towards singlet crystallization around the impurity. The distribution of K_{ij} in Fig. 2 shows also a remarkably strong modulation around the impurity.

Superconducting properties of RVB states are characterized by the singlet-pair correlations at distance \mathbf{r} , $\langle \Psi_{\text{VMC}} | \tilde{\Delta}_{\mathbf{s}+\mathbf{r}}^\dagger \tilde{\Delta}_{\mathbf{s}} | \Psi_{\text{VMC}} \rangle / \langle \Psi_{\text{VMC}} | \Psi_{\text{VMC}} \rangle$, where the operator $\tilde{\Delta}_{\mathbf{s}}^\dagger = c_{i(\mathbf{s},\uparrow)}^\dagger c_{j(\mathbf{s}+\hat{\mathbf{a}}),\downarrow}^\dagger - c_{i(\mathbf{s},\downarrow)}^\dagger c_{j(\mathbf{s}+\hat{\mathbf{a}}),\uparrow}^\dagger$ creates a singlet pair of electrons on the bond between locations \mathbf{s} and $\mathbf{s} + \hat{\mathbf{a}}$ on the lattice, $\hat{\mathbf{a}}$ being the unit vector that specifies the bond direction (along x or y). On the 8×8 cluster, we have computed pairing correlations between separate bonds for increasing bond separation. However, at the largest distance available on this cluster, the correlations have not completely reached saturation. To get a better estimation of the superconducting order parameter we have considered the 16×16 cluster and computed the pairing amplitudes $\tilde{\Delta}_{ij}$ for all bonds (i,j) within the ‘‘core’’ region,

$$\tilde{\Delta}_{i(\mathbf{s}),j(\mathbf{s}+\hat{\mathbf{a}})} = \frac{\langle \tilde{\Delta}_{\mathbf{s}} \tilde{\Delta}_{\text{bg}} \rangle}{\sqrt{\langle \tilde{\Delta}_{\text{bg}} \tilde{\Delta}_{\text{bg}} \rangle}}, \quad (3)$$

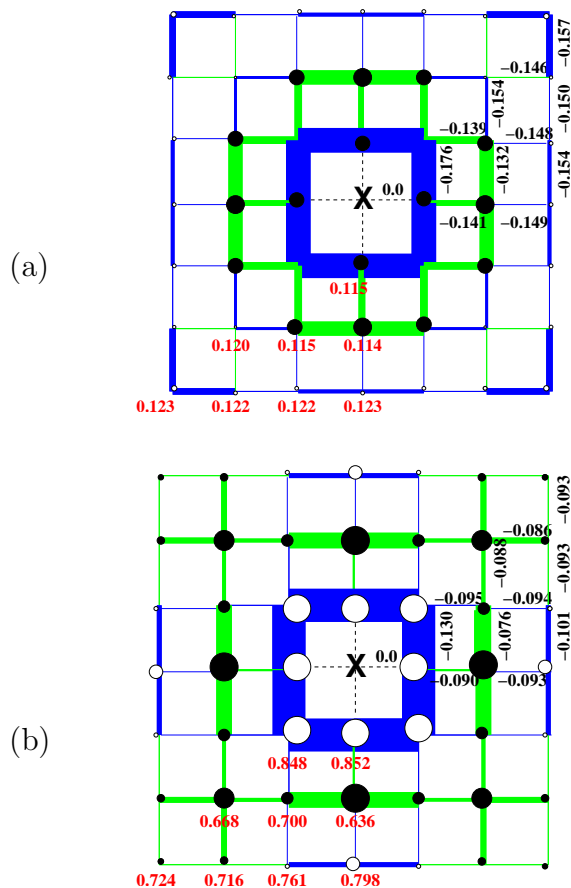


FIG. 2: (Color online.) VMC results for the GS on-site hole densities (circles) and kinetic bond amplitudes (colored segments) obtained on a 16×16 cluster. Only the central region around the impurity is shown. Diameters of circles and widths of segments scale with the *absolute value* of the *relative* differences w.r.t. the impurity-free homogenous state at the same δ_{ave} hole density (whose reference values are estimated by interpolating pure clusters with available flanking hole densities). Higher (lower) hole densities and bond magnitudes w.r.t. the homogeneous case are shown by open (filled) circles and blue (green) bonds respectively. For completeness, we also show on the plot the (bare) numerical values of the non-equivalent sites/bonds. (a) and (b) corresponds to 32 ($\delta_{\text{ave}} \simeq 0.1255$) and 20 ($\delta_{\text{ave}} \simeq 0.0784$) doped holes giving rise, for an homogeneous background, to $E_{\text{kin}}^{\text{homog}}/t = -0.1487$ and $E_{\text{kin}}^{\text{homog}}/t = -0.0941$ per bond, respectively.

where $\tilde{\Delta}_{\text{bg}}$ is a pair operator on the most remote bond in the homogeneous background. As shown in Fig. 4(a), pairing is enhanced on the dimer bonds, and is depleted around the impurity, where holes are less present.

The 16×16 cluster also allows to reduce the doping content, e.g. to 20 holes, going further into the underdoped region. Interestingly, the hole distribution around the defect is very sensitive to the doping ratio. Indeed, for doping around 12.5% (32 holes) we found that holes are slightly repelled from the bonds around the impurity. In contrast, for 7.8% doping, holes tend to concentrate

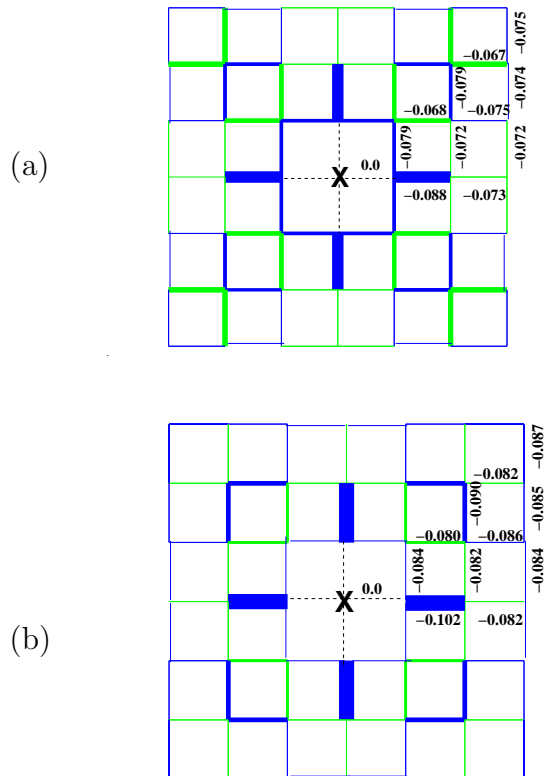


FIG. 3: (Color online.) VMC results for the GS magnetic bond amplitudes obtained on a 16×16 cluster. Same conventions and parameters as in Fig.2. (a) and (b) corresponds to 32 ($\delta_{\text{ave}} \simeq 0.1255$) and 20 ($\delta_{\text{ave}} \simeq 0.0784$) doped holes giving rise for an homogeneous background to $E_{\text{mag}}^{\text{homog}}/J = -0.074$ and $E_{\text{mag}}^{\text{homog}}/J = -0.084$ per bond, respectively.

more around the impurity site as shown in Fig. 2(b). The variational pairing $\tilde{\Delta}_{ij}$ becomes stronger on the impurity bonds suggesting the formation of a "hole pair" with the impurity *empty* site. The corresponding real space modulations of S_{ij} and $\tilde{\Delta}_{ij}$ are shown in Figs. 3(b) and 4(b).

Discussions – Let us now compare our findings to prior theoretical approaches. The first investigation of a single impurity immersed in a correlated host has been performed using Lanczos exact diagonalization of small clusters. A calculation of the local density of states¹⁸ revealed bound-states (of different orbital symmetries) in which a mobile hole is trapped by the induced impurity potential. Here, a unique mobile hole was assumed in the cluster, hence preventing real bulk pairing and giving rise to a very small doping $\sim 5\%$ in the surrounding region. Although our VMC calculations are done in a different physical range (and on much larger clusters), we find, for decreasing doping, the emergence of excess hole density around the impurity, which possibly could be consistent with a bound-state formation when $\delta \rightarrow 0$.

Metlitski and Sachdev¹⁶ have introduced a theory of valence bond solid (VBS) correlations near a single impu-

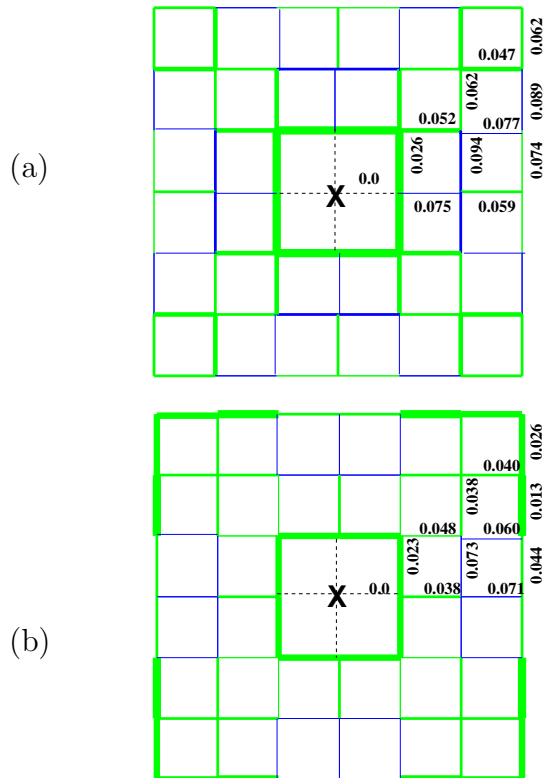


FIG. 4: (Color online.) VMC results for the pairing bond amplitudes $\bar{\Delta}_{ij}$ obtained on a 16×16 cluster. Same conventions and parameters as in Fig.2. (a) and (b) corresponds to 32 ($\delta_{\text{ave}} \simeq 0.1255$) and 20 ($\delta_{\text{ave}} \simeq 0.0784$) doped holes giving rise, for an homogeneous background, to $\Delta_{\text{bg}} \simeq 0.0787$ and $\Delta_{\text{bg}} \simeq 0.0626$, respectively.

urity in a square lattice antiferromagnet. When the system is close to a quantum transition from a magnetically ordered Néel state to a spin-gap state with long-range VBS order, a missing spin gives rise to a VBS pinwheel (or "vortex") around the impurity¹⁷. To compare with these predictions we have computed the VBS order parameter of Eq.(5) in Ref. 17. However, despite many similarities (e.g. crystallization of dimer bonds in the vicinity of the impurity), the vortex structure is not recognizable in our simulation. We hypothesize that (i) our system is probably not close enough to the critical point assumed in Ref. 16,17 and/or (ii) the VBS region develops differently in a d-wave RVB than in an AF background.

Lastly, our results are compared to the experimental STM observations around a Zn impurity in a Bi2212 cuprate superconductor shown in Ref. 11. First, we point out that GS properties have been calculated here while Ref. 11 reports spectral properties. However, since equal-time and frequency-dependent quantities are related via a simple frequency integration up to a physical cutoff (see e.g. Ref. 7 for derivation of the local hole-charge distribution from space-resolved tunneling spectra) both sets of data should reveal similarities. Indeed, like in the experiments, the patterns we found show clearly a cross-shaped symmetric structure providing evidence that (i) the theoretical modeling of the impurity as an empty site and (ii) the use of the strongly correlated t-J model to describe the bulk high-Tc superconductor are realistic.

Acknowledgments

We acknowledge support from the French Research Council (ANR). D.P. also thanks S. Sachdev for insightful discussions.

-
- ¹ F. C. Zhang and T. M. Rice, Phys. Rev. B **37**, 3759 (1988).
 - ² S. Sachdev, Rev. Mod. Phys. **75**, 913 (2003).
 - ³ P. W. Anderson, Science **235**, 1196 (1987).
 - ⁴ F. C. Zhang, C. Gros, T.M. Rice and H. Shiba, Supercond. Sci. Technol. **1**, 36 (1988).
 - ⁵ O. Fischer, M. Kugler, I. Maggio-Aprile, C. Berthod and C. Renner, Rev. Mod. Phys. **79**, 353 (2007).
 - ⁶ T. Valla, A.V. Fedorov, Jinho Lee, J.C. Davis and G.D. Gu, Science **314**, 1914 (2006).
 - ⁷ Y. Kohsaka *et al.*, Science **315**, 1380 (2007); see also J. Zaanen, *ibid.* **315**, 1372 (2007).
 - ⁸ J. M. Tranquada *et al.*, Nature (London) **375**, 561 (1995); N. B. Christensen *et al.*, Phys. Rev. Lett. **98**, 197003 (2007).
 - ⁹ P. Abbamonte *et al.*, Nature Physics **1**, 155 (2005); J.M. Tranquada *et al.*, Phys. Rev. B **78**, 174529 (2008).
 - ¹⁰ M. I. Salkola, A. V. Balatsky, and D. J. Scalapino, Phys. Rev. Lett. **77**, 1841 (1996).
 - ¹¹ S.H. Pan, E.W. Hudson, K.M. Lang, H. Eisaki, S. Uchida and J.C. Davis, Nature **403**, 746 (2000).
 - ¹² E. Dagotto, Rev. Mod. Phys. **66**, 763 (1994) and references therein.
 - ¹³ C. Gros, Phys. Rev. B **38**, 931 (1988); S. Sorella *et al.*, Phys. Rev. Lett. **88**, 117002 (2002).
 - ¹⁴ State-of-the-art VMC techniques have been recently developed to handle non-uniform correlated states; see M. Capello, M. Raczkowski and D. Poilblanc, Phys. Rev. B **77**, 224502 (2008).
 - ¹⁵ Strictly speaking, for N_h mobile holes in the cluster, the average doping of the surrounding medium is $\delta_{\text{ave}} = N_h/(L^2 - 1)$, higher than the nominal doping $\delta = N_h/L^2$.
 - ¹⁶ M.A. Metlitski and S. Sachdev, Phys. Rev. B **77**, 054411 (2008).
 - ¹⁷ R.K. Kaul, R.G. Melko, M.A. Metlitski and S. Sachdev, Phys. Rev. Lett. **101**, 187206 (2008); M.A. Metlitski and S. Sachdev, Phys. Rev. B **78**, 174410 (2008).
 - ¹⁸ D. Poilblanc, D. J. Scalapino, and W. Hanke, Phys. Rev. Lett. **72**, 884 (1994).